Unusual Formation of Point-Defect Complexes in the Ultrawide-Band-Gap Semiconductor β-Ga_2O_3

Jared M. Johnson,[1,*] Zhen Chen,[2] Joel B. Varley,[3] Christine M. Jackson,[4] Esmat Farzana,[4] Zeng Zhang,[4] Aaron R. Arehart,[4] Hsien-Lien Huang,[1] Arda Genc,[5] Steven A. Ringel,[4] Chris G. Van de Walle,[6] David A. Muller,[2,7] and Jinwoo Hwang[1,†]

[1] *Department of Materials Science and Engineering, The Ohio State University, Columbus, Ohio 43210, USA*
[2] *School of Applied and Engineering Physics, Cornell University, Ithaca, New York 14853, USA*
[3] *Lawrence Livermore National Laboratory, Livermore, California 94550, USA*
[4] *Department of Electrical and Computer Engineering, The Ohio State University, Columbus, Ohio 43210, USA*
[5] *Thermo Fisher Scientific, Hillsboro, Oregon 97124, USA*
[6] *Materials Department, University of California, Santa Barbara, California 93106, USA*
[7] *Kavli Institute at Cornell for Nanoscale Science, Cornell University, Ithaca, New York 14853, USA*

(Received 25 March 2019; published 6 November 2019)

Understanding the unique properties of ultra-wide band gap semiconductors requires detailed information about the exact nature of point defects and their role in determining the properties. Here, we report the first direct microscopic observation of an unusual formation of point defect complexes within the atomic-scale structure of β-Ga_2O_3 using high resolution scanning transmission electron microscopy (STEM). Each complex involves one cation interstitial atom paired with two cation vacancies. These divacancy-interstitial complexes correlate directly with structures obtained by density functional theory, which predicts them to be compensating acceptors in β-Ga_2O_3. This prediction is confirmed by a comparison between STEM data and deep level optical spectroscopy results, which reveals that these complexes correspond to a deep trap within the band gap, and that the development of the complexes is facilitated by Sn doping through increased vacancy concentration. These findings provide new insight on this emerging material's unique response to the incorporation of impurities that can critically influence their properties.

DOI: 10.1103/PhysRevX.9.041027 Subject Areas: Materials Science

Controlling point defects in crystalline materials can critically influence their properties, and it is therefore imperative to have well-controlled point defects to advance the materials for successful application. Point defects can be very diverse, both in terms of their structure and function. In particular, understanding the formation of point defect complexes, which may occur in response to impurity incorporation within the structure, is of great importance because of their versatile formations and influence on the materials' properties. This is particularly the case in wide-band gap semiconductors, where the intrinsic advantages of a large band gap and the possibility of high optical transparency (e.g., in transparent conductive oxides or TCOs) are severely impaired by the presence of defects. For example, the large critical field strengths that can theoretically be supported in wide-band-gap semiconductors for applications in next-generation power electronics can be ruined by the presence of defects [1], and the existence of significant deep-level defect concentrations can severely degrade the optical properties of TCOs [2]. Additionally, the presence of impurities and the formation of various types of complexes in TCOs have been suggested to contribute to the observed intrinsic n-type behavior, difficulty in p-type doping, and low doping efficiency [3–5]. What has been missing in the field is direct experimental information on the detailed atomic-scale structure of such complexes. Gaining this information is essential to exactly crosslinking theoretical predictions of complexes to measured properties of wide band gap semiconductors, which will then provide important guidance to the synthesis and doping of the material with precisely controlled properties. However, such information has been nearly unattainable because of the small (atomic-scale) nature of the defect complexes, especially when they

*Corresponding author.
johnson.6423@buckeyemail.osu.edu
†Corresponding author.
hwang.458@osu.edu

Published by the American Physical Society under the terms of the Creative Commons Attribution 4.0 International license. Further distribution of this work must maintain attribution to the author(s) and the published article's title, journal citation, and DOI.

are buried within the three-dimensional material. These challenges have led to the lack of experimental information on how the complexes incorporate within the atomic-scale structure and the inability to discover any unknown complexes that may critically affect the properties of the material.

Here, we present the first direct scanning transmission electron microscopy (STEM) observation of the unusual formation of point defect complexes within the atomic-scale structure of β-Ga_2O_3. Note that β-Ga_2O_3 is an excellent candidate for high-performance electronic, optical, power device, and sensor applications [6–15] due to its unique properties, including an ultra-wide band gap of about 4.8 eV [16], optical transparency into the ultraviolet region [17], and high breakdown voltage [18]. However, advancing the material has been hampered by the lack of a detailed understanding of the formation of point defect complexes [4,19–24] and their impact on electrical and optical properties [25–29]. Using STEM, we discovered a new type of point defect complex that involves one cation interstitial atom, which can be positioned at two of the five possible interstitial sites, paired by two cation vacancies. The structure of this unusual cation interstitial-divacancy complex is consistent with the predictions made by density functional theory (DFT). DFT also shows that this defect acts as a deep level and is the dominant compensating acceptor in β-Ga_2O_3; since β-Ga_2O_3 is n doped for most applications, this defect therefore has a crucial impact on device performance. Comparing the STEM data to deep-level optical spectroscopy (DLOS) shows that formation of the defects is enhanced by increased Sn doping, confirming the compensating-acceptor character, with a defect level at $E_C - 2.0$ eV. The present atomic-scale investigation identifies this unusual defect as the origin of a number of previously unexplained phenomena in β-Ga_2O_3 and also sheds light on this material's unique response to the incorporation of impurities that can critically influence its properties.

First, we explain the observation of interstitial defects and defect complexes in Sn-doped β-Ga_2O_3 bulk crystals (doping concentration of 8.5×10^{18} cm^{-3} yielding a carrier concentration of 8.2×10^{18} cm^{-3} [30,31]). The unit cell of monoclinic β-Ga_2O_3 contains two crystallographically different Ga (Ga_1, Ga_2) and three oxygen atom positions (O_1, O_2, O_3) as shown in Fig. 1(a). The structure is oriented along $[010]_m$, which is the orientation used throughout this study. Note that Ga_1 and Ga_2 have tetrahedral and octahedral coordination, respectively. Here, O_1 and O_2 have threefold coordination, while O_3 has fourfold coordination. Figure 1(a) also shows five potential cation interstitial sites (i_{a-e}). As will be explained in detail, these interstitial sites have been derived from both our experimental observation and DFT calculations [19,21]. A high-angle annular dark field (HAADF) STEM image (see the Appendix for details) from the $[010]_m$ Sn-doped sample of a defect-free region is shown in Fig. 1(b). As HAADF intensity depends on the atomic number, high intensity in this image mostly arises from the scattering of the Ga_1 and Ga_2 columns, while only very weak intensity is observed from O positions. Figure 2 shows the direct detection of interstitial defects and defect complexes in the same Sn-doped β-Ga_2O_3 bulk crystal. In the sample areas shown in Fig. 2(a) (left and right), significant intensities were observed in multiple interstitial sites, in addition to Ga columns that are still positioned at their regular positions. Specifically, these noticeable intensities appear in four distinct interstitial sites, termed i_{b-e} [Figs. 2(b)–2(e)]. Amongst them, the most prominent intensities were located in the i_c site [Figs. 2(c) and 2(f)]. We also note that these interstitial intensities were found to be clustered and concentrated in $\tilde{1}0$ nm^2 areas [Fig. 2(g)]. Clustering likely happens along the direction parallel to the electron beam as well, which can be evidenced by the high interstitial column intensity [e.g., Fig. 2(f)] indicating that there are likely multiple cation interstitial atoms along the column [32,33]. Previous works have identified extended defects (e.g., twin boundaries and screw dislocations) [34–36] and some atomic-scale defects [2,37] in β-Ga_2O_3, but our present data from aberration corrected STEM provide the first direct identification of the exact positions of interstitial defects.

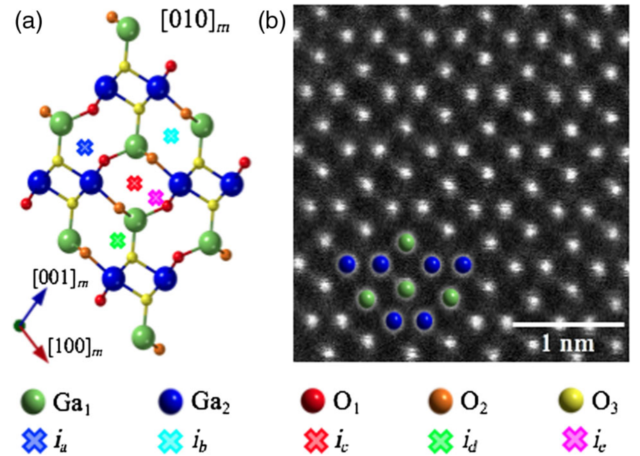

FIG. 1. Crystal structure and experimental image of β-Ga_2O_3. (a) Crystal structure of β-Ga_2O_3 along the $[010]_m$ direction with five possible interstitial sites (i_{a-e}). (b) Atomic resolution HAADF-STEM image of a $[010]_m$ Sn-doped β-Ga_2O_3 bulk crystal from a defect-free area.

Next, we identify the unique formation of point defect complexes from the HAADF-STEM intensities by directly correlating them with DFT calculations (see the Appendix for details). DFT calculations [19,20,24] have shown that cation vacancies have low formation energies under O-rich growth conditions, with tetrahedral V_{Ga}^1 being the most favorable. However, the vacancy on the tetrahedral Ga_1 site was identified as metastable; the presence of the vacancy causes a neighboring Ga atom to leave its tetrahedral site

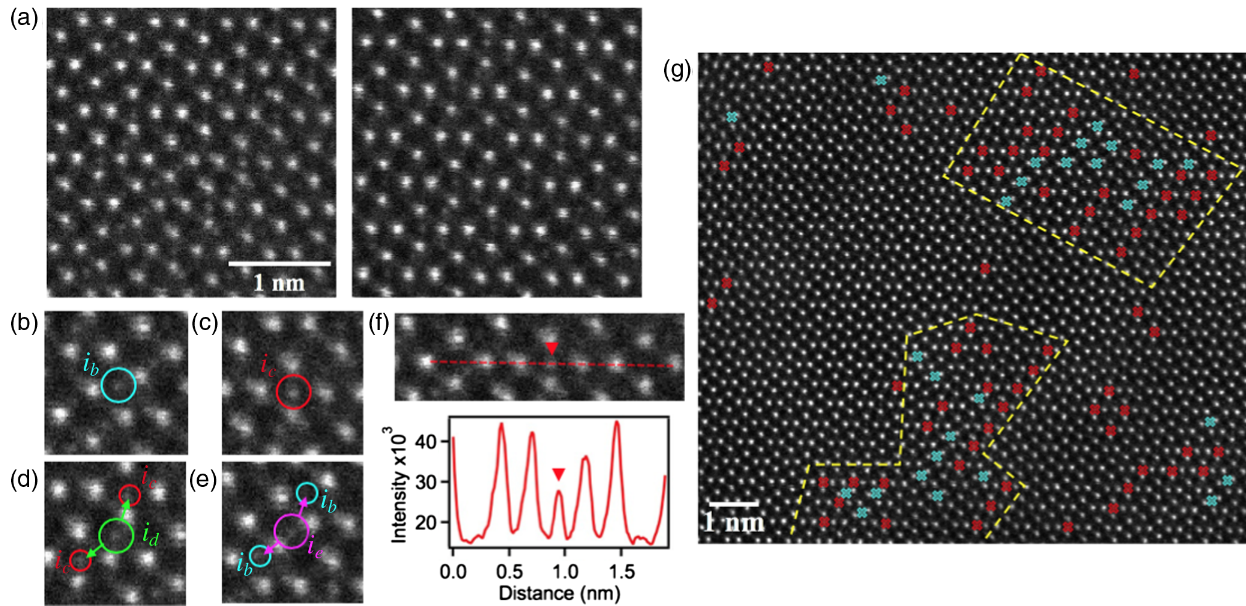

FIG. 2. Direct detection of interstitial defects in Sn-doped β-Ga_2O_3. (a) HAADF-STEM images from two regions (left and right) with clustered interstitial defects. Magnified locations from the image (a-left) with intensity located in interstitial sites (b) i_b, (c) i_c, (d) i_d, and (e) i_e are marked corresponding to Fig. 1(a). Arrows in (d) and (e) point towards accompanying interstitials in the i_b and i_c sites. (f) Intensity is evaluated across the red-dashed line, demonstrating the significant signal scattered from the cation interstitial atoms located in the i_c site (red triangle). (g) Positions of i_b (aqua mark) and i_c (red mark) interstitial atoms identified in a larger area of β-Ga_2O_3. Yellow-dashed outlined areas indicate the interstitials clustering and concentrating in areas of about 10 nm^2.

(creating a second vacancy) and move towards an interstitial site midway between the two vacancies, effectively resulting in a $2V_{Ga}^1 - Ga_i$ complex (Fig. 3). This complex is lower in energy than the isolated vacancy and acts as a deep acceptor. Figure 3(a) shows how the adjacent Ga_1 atom relaxes to the i_c site, becoming octahedrally coordinated and creating an additional V_{Ga}^1, which can be formed easily due to the relatively small energy barrier [19,21]. These DFT results have also been utilized in recent β-Ga_2O_3 defect studies using electron spin resonance [38,39] and infrared spectroscopy [40,41] to attribute the presence of proton irradiation-induced defects and implanted O-H bonds to the same point defect complexes. However, the direct confirmation of $2V_{Ga}^1 - Ga_i^c$ complexes by STEM in β-Ga_2O_3 requires the detection of not only the cation interstitial atoms (explained above) but also the vacancies in the neighboring Ga columns. Identifying a single vacancy within an atomic column may not be trivial [42]; however, the presence of several vacancies within a Ga column will decrease the overall HAADF STEM signal due to the loss of scattering from the absent Ga atoms [43]. Image simulations performed using the multislice method [44] (see the Appendix for details) confirmed that the signal increases at interstitial sites from cation interstitials and decreases at Ga_1 sites from vacancies [Figs. 3(b)–3(d)]. The loss of intensity for Ga_1 column neighboring interstitials was in fact observed in our experimental data. Individual line profiles in Fig. 3(d) illustrate the reduced intensity of Ga_1 columns adjacent to interstitials [Fig. 3(c)] compared to Ga_1 columns in a defect-free region [Fig. 3(b)]. The reduced intensity of Ga_1 columns adjacent to interstitials was substantially more significant than the overall intensity decrease in the area (including the Ga_2 columns that are not expected to be involved in the relaxation process) that may be caused by the strain [45] due to the interstitials (see Supplemental Material [46], Table S1). Image simulations indicate that the effect of electron channeling from interstitials is minimal due to the considerable gap (~0.18 nm) between the interstitials and the adjacent Ga columns. Therefore, the substantial intensity decrease, apart from the overall decrease due to strain in the Ga_1 columns adjacent to interstitials, suggests that vacancies are most likely present in those columns. Similarly, vacancy-interstitial complexes surrounding i_b sites $(2V_{Ga}^1 - Ga_i^b)$ were also observed [Figs. 3(e)–3(h)]. Quantitative comparison of atomic column intensity to the image simulation can provide information on the number of defects located within each column (e.g., Ref. [32]). Based on the experimental and simulation data (see Supplemental Material [46], Fig. S1), the estimated number of complexes within these columns is about 10 (see Supplemental Material [46] for details).

Considering the near-equilibrium growth condition of the edge-defined, film-fed growth (EFG) process used to grow these bulk crystals, the formation energy ($i_c < i_b < i_a$), predicted by DFT [19], may directly correspond to the number density of each of those point defects within

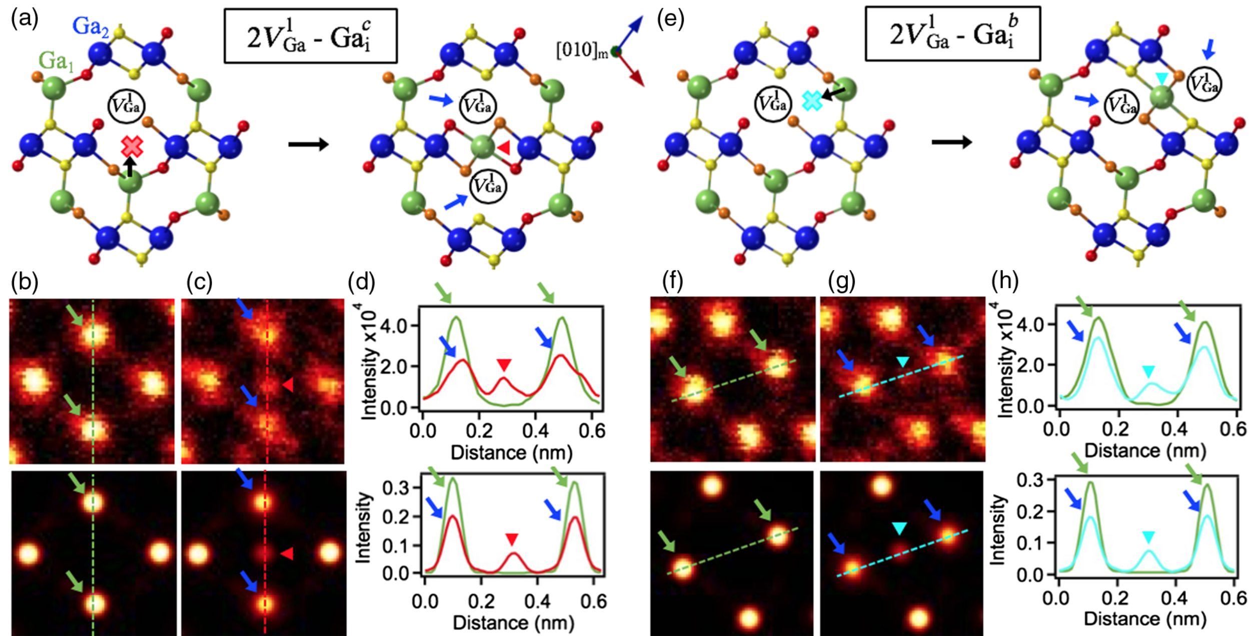

FIG. 3. Migration mechanism of V^1_{Ga} for the formation of $2V^1_{Ga} - Ga_i$ complexes. In the presence of a V^1_{Ga}, an adjacent Ga_1 relaxes into the (a) i_c or the (e) i_b site, creating an additional V^1_{Ga}. (b)–(d) Experimental and simulated HAADF images showing multiple $2V^1_{Ga} - Ga^c_i$ complexes along the $[010]_m$ direction. (d) Line profiles from a [(b), green-dashed] defect-free and [(c), red-dashed] interstitial containing experimental images show a significant reduction in Ga_1 intensity (blue arrows) from vacancies when neighboring i_c interstitials (red triangle) are compared to unperturbed Ga_1 columns (green arrows). (d) Line profiles from a [(b), green-dashed] simulated defect-free and a [(c), red-dashed] simulated 25-nm (~82 atoms) thick crystal containing 10 defect complexes located near the surface, showing similar profiles to the corresponding experimental images. (f)–(h) Similarly, experimental and simulated HAADF images show multiple $2V^1_{Ga} - Ga^b_i$ complexes along the depth direction. The simulated crystal contains 10 defect complexes located near the surface.

the material. Despite small sampling in STEM images [such as in Fig. 2(g)], the number densities of interstitials observed in the sampled region ($i_c = 1.6 \times 10^{20}$ cm^{-3} > $i_b = 3.9 \times 10^{19}$ cm^{-3} > $i_a = 0$) appear to be consistent with the energetic favorability found in the DFT calculation. In fact, we have not observed any interstitial i_a intensity above the threshold value in the sampled areas, which suggests the formation of i_a interstitials may be much less likely than i_b or i_c. Based on the analysis of images with visible interstitials [e.g., Fig. 2(g)], the estimated concentration of defect complexes is about 2×10^{20} cm^{-3} (see Supplemental Material [46] for details).

Although lesser in signal and fewer in total number, the interstitials observed in sites i_d and i_e found in Sn-doped β-Ga_2O_3 display unexplored interstitial complexes that may be important in understanding the material's properties. Interestingly, interstitial intensities in i_d and i_e sites are always observed to be accompanied by interstitial intensities in nearby i_b and i_c sites [Figs. 2(d) and 2(e)]. This may imply that $2V^1_{Ga} - Ga^{b,c}_i$ complexes may facilitate the formation of other complexes that occupy the i_d and i_e sites. The exact formation mechanism of i_d and i_e defects and their implication to the properties remain to be further explored in the near future.

The next question is then how Sn doping affects the formation of the interstitial point defect complexes shown above. In general, Sn impurities have been shown to contribute to the n-type behavior of β-Ga_2O_3, producing controllable carrier concentrations from 10^{16} up to 10^{19} cm^{-3} [30,47]. Formation energy calculations have indicated that Sn can easily be incorporated into β-Ga_2O_3 acting as a shallow donor and preferring to substitute in the octahedrally coordinated Ga_2 site [20,31]. In fact, our STEM investigation has revealed several of these Sn substitutional atoms based on the high atomic column intensity in the HAADF mode [e.g., Fig. 4(a)]. In addition to incorporating it as a substitutional dopant, Sn, when in high concentration, may promote the formation of the vacancy-interstitial complexes shown above. To verify this hypothesis, we first investigate unintentionally doped (UID) β-Ga_2O_3 (carrier concentration of 2.4×10^{17} cm^{-3} [30]) using HAADF STEM. UID β-Ga_2O_3 images revealed cation interstitials in the i_c site [Fig. 4(b)], which implies that the interstitials may also be created via the same V^1_{Ga} migration mechanism explained above. A larger sampling resulted in the conclusion that these complexes are lesser in quantity and smaller in intensity in comparison to Sn-doped β-Ga_2O_3. This result is consistent with the expectations that the incorporation of Sn donors that drive the material more

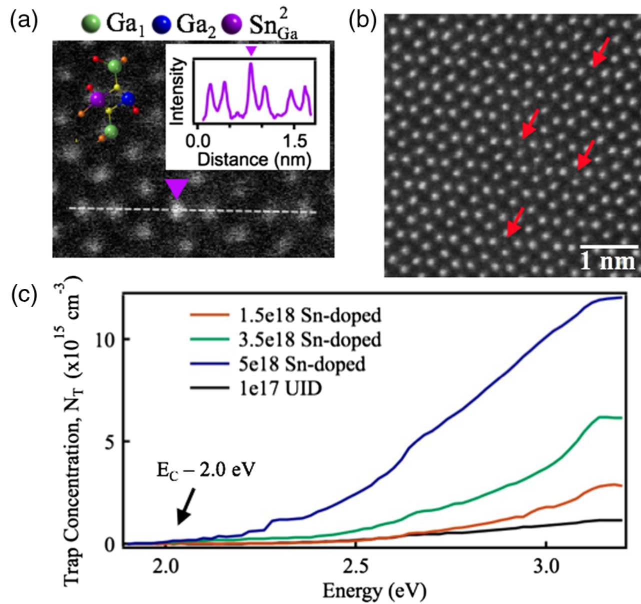

FIG. 4. STEM and DLOS results for point defects and defect complexes in β-Ga_2O_3. (a) HAADF STEM image of an atomic column containing Sn dopants (purple triangle) in $[010]_m$ bulk Sn-doped β-Ga_2O_3. The inset shows the line profile along the dashed line in the figure. (b) HAADF STEM image of UID β-Ga_2O_3 showing interstitial defects, with red arrows indicating detected Ga interstitials in the i_c sites. (c) DLOS as a function of Sn doping in bulk β-Ga_2O_3. The trap detected at $E_C - 2.0$ eV shows a positive correlation with Sn concentration.

n-type simultaneously stimulates the formation of the compensating acceptor species like the $2V_{Ga}^1 - Ga_i$ complexes through the subsequent increase in vacancy concentration [19,24]. Presuming a reduction in vacancy formation energy for increased Fermi level energy [19], Sn doping facilitates this increase in vacancy concentration through the increase in Fermi level energy. Additionally, Sn may also be incorporated as the cation interstitial, forming $2V_{Ga}^1 - Sn_i$ complexes. Its exact role will be discussed among the succeeding results.

DLOS can reveal the rich spectrum of defect states throughout the large band gap [29], by using monochromatic incident light as a function of energy to photo-emit trapped carriers to a band edge, which enables the determination of energy levels, concentrations, and optical cross sections of deep states (see the Appendix for details [29,48,49]). Accompanying our STEM results and DFT calculations, the DLOS results are consistent with the role of Sn dopant concentration and the number of vacancy-interstitial complexes present. Most importantly, the concentration of the trap detected at $E_C - 2.0$ eV shows a positive correlation with Sn concentration [Fig. 4(c)], and the trap has been shown to act as a deep acceptor [50]. This defect behavior is consistent with the electronic state of the $2V_{Ga}^1 - Ga_i$ complexes predicted by DFT, where levels associated with the expected $\varepsilon(-2/-3)$ charge-state transition levels have been predicted to fall between $E_C - 1.9$ and $E_C - 2.5$ eV [19,24]. The analogous $\varepsilon(-/-2)$ levels calculated for the $2V_{Ga}^1 - Sn_i$ complexes are found to be in a similar energy range, at $E_C - 2.34$ and $E_C - 2.89$ eV for the i_b and i_c sites, respectively. The apparent defect concentrations obtained from DLOS represent the average over large areas (as opposed to the relatively smaller area observations of STEM) and are limited by the finite time response of the defects [50]. Nonetheless, the positive correlation between the DLOS detected trap and doping concentration, along with the detection of this trap in UID β-Ga_2O_3, directly coincides with the observation of interstitials by STEM imaging, which affirms the physical source of the $E_C - 2.0$ eV defect state to be the divacancy-interstitial complex.

It would be highly valuable to be able to distinguish whether the observed entities are $2V_{Ga}^1 - Ga_i$ (spatially separated from donor impurities) or actual $2V_{Ga}^1 - Sn_i$ complexes since it could help identify strategies for controlling the compensating acceptor. The proposed $2V_{Ga}^1 - Sn_i$ acceptor complexes have also been suggested to contribute to compensation in Sn-doped β-Ga_2O_3 [51]. Our calculations show that these complexes can readily form when V_{Ga} are nearby (calculated barriers less than 0.3 eV for an Sn_{Ga}^1 to be displaced to octahedrally coordinated interstitials adjacent to V_{Ga1}) and are quite stable, with calculated binding energies of at least 1.4 eV relative to isolated V_{Ga} and Sn_{Ga} species (see Supplemental Material [46], Fig. S2). However, we expect that these complexes would need to form during growth, as Sn is not expected to be appreciably incorporated on the tetrahedral sites, which is a prerequisite for their formation postgrowth [20]. As mentioned above, determining the species of cation interstitials in Sn-doped β-Ga_2O_3 via HAADF-STEM is difficult because variations in number and location make Ga and Sn interstitials indistinguishable (see Supplemental Material [46], Fig. S1). However, because DLOS results reveal the same trap ($E_C - 2.0$ eV) in both UID and Sn-doped β-Ga_2O_3 while DFT calculations predict different electronic states for $2V_{Ga}^1 - Ga_i$ and $2V_{Ga}^1 - Sn_i$ complexes, the observed compensating acceptors correlate with native $2V_{Ga}^1 - Ga_i$ complexes.

In summary, the STEM results provide the first observation of unusual divacancy-cation interstitial complexes, and the structure of the identified complexes matches with DFT predictions that classify them as compensating acceptors. DLOS results further validate the formation of these complexes, as the detected $E_C - 2.0$ eV defect state shows a positive correlation with Sn doping. Sn was determined to facilitate the divacancy-interstitial complex development by increasing the Fermi level energy and subsequently increasing the vacancy concentration. These STEM results provide new important insight on the material's unique response to the impurity incorporation that can significantly affect their properties, which can ultimately offer important

guidance to the development of growth and doping of TCOs for novel applications. The observed complex is, in essence, a low-symmetry configuration of a cation vacancy. It will be highly interesting to explore, using computational theory and/or microscopy, whether vacancies in other materials can also spontaneously undergo such symmetry-breaking distortions.

ACKNOWLEDGMENTS

S. A. R., C. V., and J. H. acknowledge support by the Department of Defense, Air Force Office of Scientific Research GAME MURI Program (Grant No. FA9550-18-1-0479). This work was performed in part at the Cornell PARADIM Electron Microcopy Facility, as part of the Materials for Innovation Platform Program, which is supported by the NSF under Grant No. DMR-1539918 with additional infrastructure support by Grants No. DMR1719875 and No. DMR-1429155. S. A. R. acknowledges additional support from the DTRA Grant No. HDTRA1-17-1-0034. DFT work was partially performed under the auspices of the U.S. DOE by Lawrence Livermore National Laboratory under Contract No. DE-AC52-07NA27344, and partially supported by the Critical Materials Institute, an Energy Innovation Hub funded by the U.S. DOE, Office of Energy Efficiency and Renewable Energy, Advanced Manufacturing Office.

APPENDIX: METHODS

The $(\bar{2}01)$ Sn-doped and unintentionally doped (UID) β-Ga_2O_3 bulk crystals used in this investigation were fabricated by the edge-defined, film-fed growth (EFG) process by the Tamura Corporation. The Sn-doped and UID samples have carrier concentrations of 8.2×10^{18} cm^{-3} and 2.4×10^{17} cm^{-3}, respectively. Crystal orientations such as the $[010]_m$ and $[001]_m$ yield advantageous viewing directions for point defect imaging due to the large atomic spacings. Cross-sectional $[010]_m$ TEM samples were prepared using a focused ion beam (FIB). As atomic resolution imaging of $[010]_m$ β-Ga_2O_3 requires thin, clean samples, we further milled TEM samples using a low-energy (500-eV) ion mill (Fischione Nanomill). The final thickness of the TEM foils was determined by position-averaged convergent beam electron diffraction to be about 25 nm [32,52], meaning each gallium column contains about 80 atoms along the depth direction. STEM was then performed using aberration-corrected Thermo Fisher Scientific Titan Themis STEM instruments, all operated at 300 kV.

All STEM HAADF image simulations were performed using the multislice algorithm [44]. For each image simulation of randomly distributed defect complexes, ten random arrangements were simulated and then averaged to increase statistical reliability. Thermal vibrations were ignored as their contribution to column intensity is minimal. The image simulations used aberration parameters of our probe-corrected FEI Titan STEM ($Cs_3 = 0.002$ mm, $Cs_5 = 1.0$ mm) with a 20.0-mrad convergence half-angle at an acceleration voltage of 300 kV.

The DFT atomistic simulations of the vacancy complex energetics were based on hybrid functional calculations performed using the same methodology as described in Ref. [24]. Specifically, the vacancy and vacancy complexes were modeled within a 160-atom supercell representation of bulk β-Ga_2O_3, where corrections to the formation energies of charged defects owing to image-charge interactions were included as detailed in Ref. [24]. Migration barriers were computed between linearly interpolated structures and thus offer upper bounds to the real barriers.

DLOS was performed on Ni/Ga_2O_3 Schottky diodes on four different β-Ga_2O_3 substrates from Tamura: $n\sim 1\times10^{17}$ cm^{-3} UID (010), $n\sim 1.5\times10^{18}$ cm^{-3} Sn-doped (−201), $n\sim 3.5\times10^{18}$ cm^{-3} Sn-doped (010), $n\sim 5\times 10^{18}$ cm^{-3} Sn-doped (010). Carrier concentrations on these samples were confirmed by C-V measurements. DLOS utilizes monochromatic subbandgap light to observe optically stimulated photoemission transients as a function of incident light energy. Here, light from a 1000-W Xe lamp was dispersed through a high-resolution monochromator to provide incident light from 1.2 eV to 5.0 eV in 0.02-eV steps, and photoemission transients were measured for 300 seconds.

[1] M. A. Reshchikov and H. Morkoc, *Luminescence Properties of Defects in GaN*, J. Appl. Phys. **97**, 061301 (2005).
[2] Z. Galazka, R. Uecker, K. Irmscher, M. Albrecht, D. Klimm, M. Pietsch, M. Brützam, R. Bertram, S. Ganschow *et al.*, *Czochralski Growth and Characterization of* β-Ga_2O_3 *Single Crystals*, Cryst. Res. Technol. **45**, 1229 (2010).
[3] E. G. Víllora, K. Shimamura, Y. Yoshikawa, T. Ujiie, and K. Aoki, *Electrical Conductivity and Carrier Concentration Control in* β-Ga_2O_3 *by Si Doping*, Appl. Phys. Lett. **92**, 202120 (2008).
[4] J. B. Varley, A. Janotti, C. Franchini, and C. G. Van, *de Walle, Role of Self-Trapping in Luminescence and p-Type Conductivity of Wide-Band-Gap Oxides*, Phys. Rev. B **85**, 081109(R) (2012).
[5] K. Sasaki, M. Higashiwaki, A. Kuramata, T. Masui, and S. Yamakoshi, *Si-Ion Implantation Doping in* β-Ga_2O_3 *and Its Application to Fabrication of Low-Resistance Ohmic Contacts*, Appl. Phys. Express **6**, 086502 (2013).
[6] F. Shizuo, *Wide-Bandgap Semiconductor Materials: For Their Full Bloom*, Jpn. J. Appl. Phys. **54**, 030101 (2015).
[7] M. Higashiwaki, A. Kuramata, H. Murakami, and Y. Kumagai, *Current Status of* Ga_2O_3 *Power Devices*, Jpn. J. Appl. Phys. **55**, 1202A1 (2016).
[8] M. Higashiwaki, A. Kuramata, H. Murakami, and Y. Kumagai, *State-of-the-Art Technologies of Gallium Oxide Power Devices Current Status of* Ga_2O_3 *Power Devices*, J. Phys. D **50**, 333002 (2017).
[9] M. Higashiwaki, K. Sasaki, H. Murakami, Y. Kumagai, A. Koukitu, A. Kuramata, T. Masui, and S. Yamakoshi, *Recent*

Progress in Ga_2O_3 *Power Devices*, Semicond. Sci. Technol. **31**, 034001 (2016).

[10] S. I. Stepanov, V. I. Nikolaev, V. E. Bougrov, and A. E. Romanov, *Gallium Oxide: Properties and Applications—A Review*, Rev. Adv. Mater. Sci. **44**, 63 (2016), https://pdfs.semanticscholar.org/227c/d22af58a530db8fc4e4cc8cb74d85840cc0e.pdf.

[11] M. Higashiwaki, K. Sasaki, T. Kamimura, M. H. Wong, and D. Krishnamurthy, *Depletion-Mode* Ga_2O_3 *Metal-Oxide-Semiconductor Field-Effect Transistors on* β-Ga_2O_3 *(010) Substrates and Temperature Dependence of Their Device Characteristics*, Appl. Phys. Lett. **103**, 123511 (2013).

[12] M. Orita, H. Ohta, M. Hirano, and H. Hosono, *Deep-Ultraviolet Transparent Conductive* β-Ga_2O_3 *Thin Films*, Appl. Phys. Lett. **77**, 4166 (2000).

[13] M. Higashiwaki, K. Sasaki, A. Kuramata, T. Masui, and S. Yamakoshi, *Development of Gallium Oxide Power Devices*, Phys. Status Solidi Appl. Mater. Sci. **211**, 21 (2014).

[14] M. Kim, J. H. Seo, U. Singisetti, and Z. Ma, *Recent Advances in Free-Standing Single Crystalline Wide Band-Gap Semiconductors and Their Applications: GaN, SiC, ZnO,* β-Ga_2O_3*, and Diamond*, J. Mater. Chem. C **5**, 8338 (2017).

[15] M. A. Mastro, A. Kuramata, J. Calkins, J. Kim, F. Ren, and S. J. Pearton, *Perspective—Opportunities and Future Directions for* Ga_2O_3, ECS J. Solid State Sci. Technol. **6**, P356 (2017).

[16] H. H. Tippins, *Optical Absorption and Photoconductivity in the Band Edge of* β-Ga_2O_3, Phys. Rev. **140**, A316 (1965).

[17] N. Ueda, H. Hosono, R. Waseda, and H. Kawazoe, *Synthesis and Control of Conductivity of Ultraviolet Transmitting* β-Ga_2O_3 *Single Crystals*, Appl. Phys. Lett. **70**, 3561 (1997).

[18] M. Higashiwaki, K. Sasaki, A. Kuramata, T. Masui, and S. Yamakoshi, *Gallium Oxide (*Ga_2O_3*) Metal-Semiconductor Field-Effect Transistors on Single-Crystal* β-Ga_2O_3 *(010) Substrates*, Appl. Phys. Lett. **100**, 013504 (2012).

[19] J. B. Varley, H. Peelaers, A. Janotti, and C. G. Van de Walle, *Hydrogenated Cation Vacancies in Semiconducting Oxides*, J. Phys. Condens. Matter **23**, 334212 (2011).

[20] J. B. Varley, J. R. Weber, A. Janotti, and C. G. Van de Walle, *Oxygen Vacancies and Donor Impurities in* β-Ga_2O_3, Appl. Phys. Lett. **97**, 142106 (2010).

[21] A. Kyrtsos, M. Matsubara, and E. Bellotti, *Migration Mechanisms and Diffusion Barriers of Vacancies in* Ga_2O_3, Phys. Rev. B **95**, 245202 (2017).

[22] H. Li and J. Robertson, *Behaviour of Hydrogen in Wide Band Gap Oxides*, J. Appl. Phys. **115**, 203708 (2014).

[23] T. Zacherle, P. C. Schmidt, and M. Martin, *Ab Initio Calculations on the Defect Structure of* β-Ga_2O_3, Phys. Rev. B **87**, 235206 (2013).

[24] M. E. Ingebrigtsen, A. Y. Kuznetsov, B. G. Svensson, G. Alfieri, A. Milhaila, U. Badstubner, A. Perron, L. Vines, and J. B. Varley, *Impact of Proton Irradiation on Conductivity and Deep Level Defects in* β-Ga_2O_3, APL Mater. **7**, 022510 (2019).

[25] K. Iwaya, R. Shimizu, H. Aida, T. Hashizume, and T. Hitosugi, *Atomically Resolved Silicon Donor States of* β-Ga_2O_3, Appl. Phys. Lett. **98**, 142116 (2011).

[26] B. E. Kananen, L. E. Halliburton, K. T. Stevens, G. K. Foundos, and N. C. Giles, *Gallium Vacancies in* β-Ga_2O_3 *Crystals*, Appl. Phys. Lett. **110**, 202104 (2017).

[27] E. Korhonen, F. Tuomisto, D. Gogova, G. Wagner, M. Baldini, Z. Galazka, R. Schewski, and M. Albrecht, *Electrical Compensation by Ga Vacancies in* Ga_2O_3 *Thin Films*, Appl. Phys. Lett. **106**, 242103 (2015).

[28] A. T. Neal, S. Mou, S. Rafique, H. Zhao, E. Ahmadi, J. S. Speck, K. T. Stevens, J. D. Blevins, D. B. Thomson *et al.*, *Donors and Deep Acceptors in* β-Ga_2O_3, Appl. Phys. Lett. **113**, 062101 (2018).

[29] Z. Zhang, E. Farzana, A. R. Arehart, and S. A. Ringel, *Deep Level Defects throughout the Bandgap of (010)* β-Ga_2O_3 *Detected by Optically and Thermally Stimulated Defect Spectroscopy*, Appl. Phys. Lett. **108**, 052105 (2016).

[30] A. Kuramata, K. Koshi, S. Watanabe, Yu Yamaoka, T. Masui and S. Yamakoshi, *High-Quality* β-Ga_2O_3 *Single Crystals Grown by Edge-Defined Film-Fed Growth*, Jpn. J. Appl. Phys. **55**, 1202A2 (2016).

[31] S. C. Siah, R. E. Brandt, K. Lim, L. T. Schelhas, R. Jaramillo, M. D. Heinemann, D. Chua, J. Wright, J. D. Perkins *et al.*, *Dopant Activation in Sn-Doped* Ga_2O_3 *Investigated by X-Ray Absorption Spectroscopy*, Appl. Phys. Lett. **107**, 252103 (2015).

[32] J. Hwang, J. Y. Zhang, A. J. D'Alfonso, L. J. Allen, and S. Stemmer, *Three-Dimensional Imaging of Individual Dopant Atoms in* $SrTiO_3$, Phys. Rev. Lett. **111**, 266101 (2013).

[33] P. M. Voyles, D. A. Muller, J. L. Grazul, P. H. Citrin, and H.-J. L. Gossmann, *Atomic-Scale Imaging of Individual Dopant Atoms and Clusters in Highly n-Type Bulk Si*, Nature (London) **416**, 826 (2002).

[34] K. Nakai, T. Nagai, K. Noami, and T. Futagi, *Characterization of Defects in* β-Ga_2O_3 *Single Crystals*, Jpn. J. Appl. Phys. **54**, 051103 (2015).

[35] A. Fiedler, R. Schewski, M. Baldini, Z. Galazka, G. Wagner, M. Albrecht, and K. Irmscher, *Influence of Incoherent Twin Boundaries on the Electrical Properties of* β-Ga_2O_3 *Layers Homoepitaxially Grown by Metal-Organic Vapor Phase Epitaxy*, J. Appl. Phys. **122**, 165701 (2017).

[36] S. W. Kaun, F. Wu, and J. S. Speck, $\beta-(Al_xGa_{1-x})_2O_3/$ Ga_2O_3 *(010) Heterostructures Grown on*$\beta-Ga_2O_3$ *(010) Substrates by Plasma-Assisted Molecular Beam Epitaxy*, J. Vac. Sci. Technol. **33**, 041508 (2015).

[37] P. Ravadgar, R.-H. Horng, S.-D. Yao, H.-Y. Lee, B.-R. Wu, S.-L. Ou, and L.-W. Tu, *Effects of Crystallinity and Point Defects on Optoelectronic Applications of* β-Ga_2O_3 *Epilayers*, Opt. Express **21**, 24599 (2013).

[38] D. Skachkov, W. R. L. Lambrecht, H. J. von Bardeleben, U. Gerstmann, Q. D. Ho, and P. Deak, *Computational Identification of Ga-Vacancy Related Electron Paramagnetic Resonance Centers in* β-Ga_2O_3, J. Appl. Phys. **125**, 185701 (2019).

[39] H. J. von Bardeleben, S. Zhou, U. Gerstmann, D. Skachkov, W. R. L. Lambrecht, Q. D. Ho, and P. Deak, *Proton Irradiation Induced Defects in—*Ga_2O_3*: A Combined EPR and Theory Study*, APL Mater. **7**, 022521 (2019).

[40] Y. Qin, M. Stavola, W. B. Fowler, P. Weiser, and S. J. Pearton, *Hydrogen Centers in* β-Ga_2O_3*: Infrared Spectroscopy and Density Functional Theory*, ECS J. Solid State Sci. Technol. **8**, Q3103 (2019).

[41] P. Weiser, M. Stavola, W. B. Fowler, Y. Qin, and S. Pearton, *Structure and Vibrational Properties of the*

Dominant O-H Center in β-Ga_2O_3, Appl. Phys. Lett. **112**, 232104 (2018).

[42] J. M. Johnson, S. Im, W. Windl, and J. Hwang, *Three-Dimensional Imaging of Individual Point Defects Using Selective Detection Angles in Annular Dark Field Scanning Transmission Electron Microscopy*, Ultramicroscopy **172**, 17 (2017).

[43] H. Kim, J. Y. Zhang, S. Raghavan, and S. Stemmer, *Direct Observation of Sr Vacancies in* $SrTiO_3$ *by Quantitative Scanning Transmission Electron Microscopy*, Phys. Rev. X **6**, 041063 (2016).

[44] E. J. Kirkland, R. F. Loane, and J. Silcox, *Simulation of Annular Dark Field Stem Images Using a Modified Multislice Method*, Ultramicroscopy **23**, 77 (1987).

[45] D. A. Muller, N. Nakagawa, A. Ohtomo, J. L. Grazul, and H. Y. Hwang, *Atomic-Scale Imaging of Nanoengineered Oxygen Vacancy Profiles in* $SrTiO_3$, Nature (London) **430**, 657 (2004).

[46] See Supplemental Material at http://link.aps.org/supplemental/10.1103/PhysRevX.9.041027 for a statistical analysis of column intensities, multislice simulations, and formation energy calculations.

[47] M. Baldini, M. Albrecht, A. Fiedler, K. Irmscher, and R. Schewski, *Si- and Sn-Doped Homoepitaxial* β-Ga_2O_3 *Layers Grown by MOVPE on (010)-Oriented Substrates*, ECS J. Solid State Sci. Technol. **6**, Q3040 (2017).

[48] A. Hierro, D. Kwon, S. A. Ringel, M. Hansen, J. S. Speck, U. K. Mishra, and S. P. Denbaars, *Optically and Thermally Detected Deep Levels in n-Type Schottky and GaN Diodes*, Appl. Phys. Lett. **76**, 3064 (2000).

[49] E. Farzana, Z. Zhang, P. K. Paul, A. R. Arehart, and S. A. Ringel, *Influence of Metal Choice on (010)* β-Ga_2O_3 *Schottky Diode Properties*, Appl. Phys. Lett. **110**, 202102 (2017).

[50] E. Farzana, M. F. Chaiken, T. E. Blue, A. R. Arehart, and S. A. Ringel, *Impact of Deep Level Defects Induced by High Energy Neutron Radiation in* β-Ga_2O_3, APL Mater. **7**, 022502 (2019).

[51] S. Lany, *Defect Phase Diagram for Doping of* Ga_2O_3, APL Mater. **6**, 046103 (2018).

[52] J. M. LeBeau, S. D. Findlay, L. J. Allen, and S. Stemmer, *Position Averaged Convergent Beam Electron Diffraction: Theory and Applications*, Ultramicroscopy **110**, 118 (2010).